Negative-hyperon production in high-energy proton interactions*

V. Hungerbühler,† R. Majka, J. N. Marx, P. Némethy, J. Sandweiss, W. Tanenbaum,‡ and W. J. Willis§
Yale University, New Haven, Connecticut 06520

M. Atac, S. Ecklund, P. J. Gollon, J. Lach, J. MacLachlan, A. Roberts, R. Stefanski, and D. Theriot
Fermi National Accelerator Laboratory, Batavia, Illinois 60510‖

C. L. Wang
Brookhaven National Laboratory, Upton, New York 11973¶
(Received 6 March 1975)

Momentum spectra for forward Σ^- and Ξ^- production by protons on beryllium are presented. Σ^- production data for two primary proton momenta are compared to test scaling of the invariant cross section. In addition, the observed single-particle momentum distributions are compared with single-particle spectra from other inclusive reactions initiated by protons.

I. INTRODUCTION

We report a measurement of the momentum spectra of Σ^- and Ξ^- hyperons produced by high-energy proton interactions on beryllium. The experiment was performed using the Yale-BNL-Fermilab hyperon beam at the Brookhaven National Laboratory Alternating Gradient Synchrotron (AGS). The production cross sections were measured for secondary momenta between 17 and 26.0 GeV/c for incident proton momenta of 25.8 and 29.4 GeV/c in the case of Σ^- and 29.4 GeV/c in the case of Ξ^-. In addition, a single Ω^- candidate produced from 29.4-GeV/c protons was observed at a secondary momentum of 20.5 GeV/c. We compare the Σ^- and Ξ^- momentum distribution with the inclusive spectra of other particles produced in proton-initiated reactions. The results for Σ^- production have been previously reported in Ref. 1.

II. THE HYPERON BEAM AND DETECTION APPARATUS

Figure 1 is a schematic representation of the hyperon beam and detection apparatus, which is described in greater detail elsewhere.[2] A slowly extracted proton beam of about 10^{11} protons per AGS pulse interacts in a $0.66\times0.66\times25.4$-cm^3 Be target. The target is followed by a curved, shielded magnetic channel 436.9 cm long with an 8.4° bend, which accepts negatively charged secondaries produced at 0° with respect to the incident proton beam. This length is sufficient to shield the downstream detectors from hadronic backgrounds produced in the target, while limiting decay losses of Σ^- and Ξ^- to an acceptable level. The channel has a solid-angle acceptance of 22 μsr, and a momentum acceptance of approximately 10% (FWHM). A scintillation-counter telescope viewing the production target at 146° is used to monitor the interaction rate.

The inside walls of the second half of the channel are aluminized and tapered. When filled with Freon gas[3] at atmospheric pressure, the channel acts as a threshold Čerenkov counter ($\check{C}_B$). Čerenkov light is reflected from a 5-μm-thick pellicle mirror located at the downstream end of the channel onto a 56 DVP photomultiplier tube. Light beam particles ($\pi^-, K^-, \bar{p}$), which form the most serious potential background, are thus tagged and rejected with an efficiency of over 99.9%. This tagging scheme is reinforced by a scintillation counter, V_π, located at the downstream end of the apparatus, whose function is to veto stable beam particles.

The position and direction of the beam particles are measured by high-resolution (100-μm) magnetostrictive-readout spark chambers[4] placed immediately after the beam channel. These chambers operate with small gaps (1.2 mm) and at high pressure (10 atm). They yield measurements of the hyperon momentum to ± 1% and direction to ± 0.5 mrad with minimal decay loss in the spark chambers. The high-pressure chambers are sandwiched between small beam-defining scintillation counters (B) and are followed by a hole veto counter (V_H) and by a 2.9-m-long shielded decay region.

Downstream from the decay region are two magnet–spark-chamber spectrometers, the first for analyzing the light decay products of hyperon decays (π^-, K^-, e^-) and the second for analyzing the high-momentum decay proton from hyperon decays with a Λ^0 in the final state. These momenta are measured to an accuracy of better than 5%. A scintillation-counter hodoscope (S) is located between the spectrometers on the negative side of the neutral beam line. A 0.71-m-long atmos-

Copyright © 1975 by The American Physical Society.

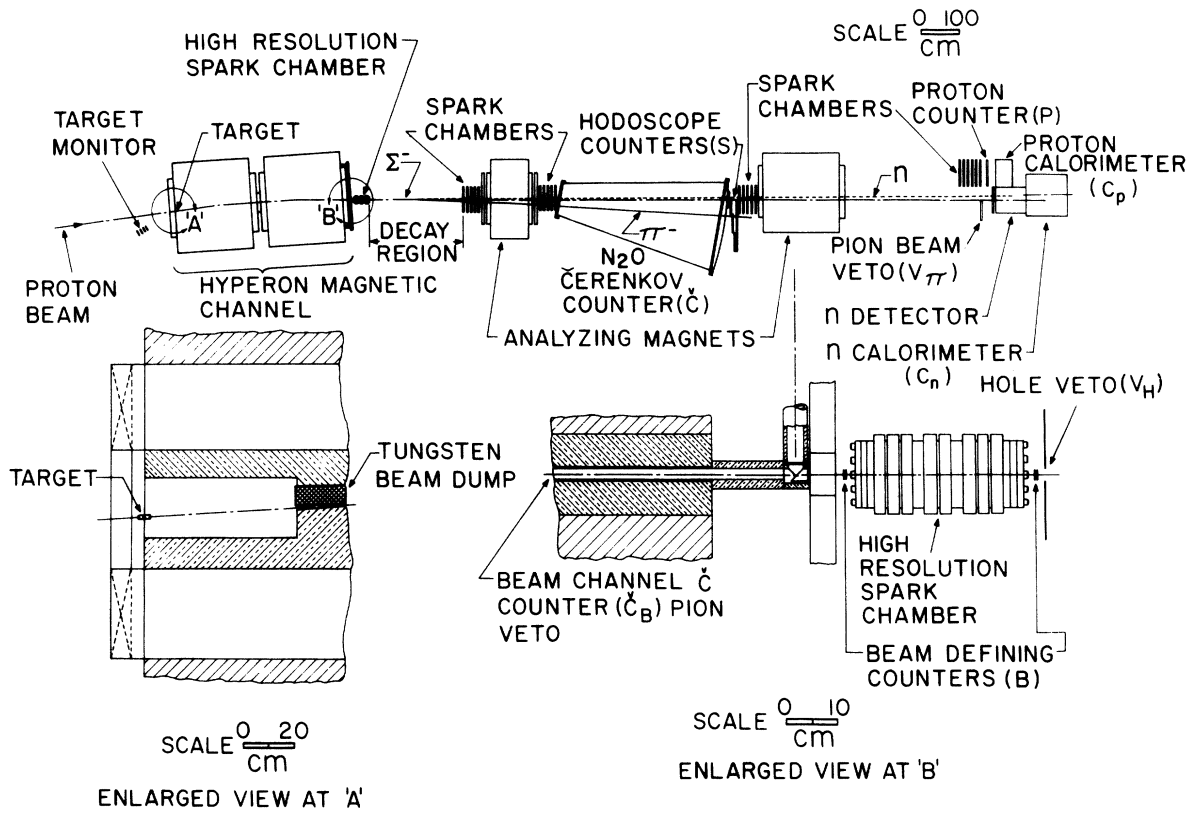

FIG. 1. Schematic diagram of the high-energy hyperon beam and detection apparatus at the BNL AGS.

pheric pressure threshold Čerenkov counter (Č), located between the spectrometer magnets, is used to separate kaons from pions in the studies of Ω^- production.

Two total-absorption scintillation-counter iron-plate calorimeters are located after the second spectrometer magnet. A minimum calorimeter pulse-height requirement in the trigger allows muons to be separated from high-energy hadrons. We use the calorimeter on the neutral beam line (C_n) to identify fast neutrons and the calorimeter on the positive side (C_p) to identify high-energy protons from Λ^0 decay. The pulse-height information from the calorimeters was not used in the analysis.

III. DATA COLLECTION

We report on Σ^- data taken with the trigger (see Fig. 1)

$$\bar{Č}_B \cdot B \cdot \bar{V}_H \cdot S \cdot \bar{V}_\pi \cdot C_n ,$$

where C_n denotes a pulse height in the neutron calorimeter greater than that produced by background muons. This trigger selects events with a massive, unstable beam particle, a slow negative particle following the first spectrometer magnet, and a fast neutron following the second spectrometer magnet. This is the signature for the decay

$$\Sigma^- \to n\pi^- .$$

The background in this trigger is less than 0.5%, consisting mainly of beam pions which are missed by the beam Čerenkov veto and by the stable-beam-particle veto, V_π.

These data were collected in two series of runs, one for each primary proton momentum (25.8 and 29.4 GeV/c). Within each series, individual runs were taken by varying the magnetic field in the shielded channel, thus changing the average hyperon momentum. Hyperon momenta from 17.0 to 26.0 GeV/c were studied in approximately 1-GeV/c steps. During the data runs at 25.8-GeV/c primary proton momentum, the rate of beam pion triggers ($\bar{Č}_B \cdot B \cdot \bar{V}_H \cdot S \cdot V_\pi$) was recorded to provide the normalization for the hyperon fluxes. For the 29.4-GeV/c runs, the apparatus was

triggered on beam pions at a rate prescaled to a convenient level. These events, which consist of a single track in each of the relevant spark chambers, as do the Σ^- events, were analyzed along with the Σ^- candidates. This procedure yields a Σ^-/π^- production ratio which is independent of spark-chamber performance.

Ξ^- data were taken at an incident proton momentum of 29.4 GeV/c with the trigger $\bar{\bar{C}}_B \cdot B \cdot \bar{V}_H \cdot S \cdot \bar{V}_\pi \cdot C_p$, where C_p denotes a pulse height in the proton calorimeter greater than that produced by background muons. This trigger selects a massive unstable beam particle, one or more slow negative particles following the first spectrometer magnet, and a fast proton following the second spectrometer, and is the signature for

$$\Xi^- \rightarrow \Lambda^0 \pi^- \searrow \pi^- p \,.$$

In order to search for Ω^- particles, a separate lengthy run was taken with an incident proton momentum of 29.4 GeV/c and a secondary momentum of 20.5 GeV/c. During this run the threshold Čerenkov counter located between the spectrometer magnets was filled with nitrous oxide (N_2O) and used to separate kaons from pions in the momentum range 5 to 12 GeV/c. The primary trigger for this run was $\bar{\bar{C}}_B \cdot B \cdot \bar{V}_H \cdot \bar{\bar{C}} \cdot S \cdot \bar{V}_\pi \cdot C_p$, which is the signature for the decay

$$\Omega^- \rightarrow \Lambda^0 K^- \searrow \pi^- p \,.$$

IV. ANALYSIS

The first phase of the data analysis served to extract the numbers of detected beam particles ($\pi^-, \Sigma^-, \Xi^-, \Omega^-$) in the appropriate trigger categories for each run. All triggers were subject to to the same initial criteria in order to define particles in the beam channel phase space. The high-resolution spark chamber was required to have a single track which could be extrapolated in the vertical projection to within 0.8 cm of the production target. In the horizontal plane, the beam track was required to be inside of the beam channel when the nominal beam momentum and the assumption of a point production target were used to project back to the channel midpoint. These criteria eliminated particles produced in the channel walls and decays upstream from the high-resolution chambers.

Next, we required a minimal topology in the spark chambers associated with the magnetic spectrometers. For π^- and Σ^- triggers, we required at least one good track in the chambers before and after the first spectrometer magnet. For Ξ^- and Ω^- triggers, at least three good tracks were required in the chambers before and after the first spectrometer and at least one good track in the chambers before and after the second spectrometer. In addition, at least one track through the second spectrometer was required to have the curvature of a positive particle (presumed to be the proton from $\Lambda^0 \rightarrow \pi^- p$). The spark-chamber clusters have ten planes and a good track was defined as having at least eight sparks on a straight line with a χ^2/(degree of freedom) < 8.

Candidate tracks associated with the real event were separated from background tracks by topological requirements. In all cases the projected distance of closest approach between the beam track and a track in the chambers before the first spectrometer was required to be less than 0.6 cm. An additional topological constraint was imposed on this intersection. For π^- candidates the kink angle was required to be less than 3 mr, while for hyperon candidates it was required to be greater than 9 mr. This requirement ensures the presence of a decay, where appropriate, and allows the definition of a fiducial volume in the decay region by eliminating events whose decay angle is too small to allow adequate definition of the decay point along the beam direction. In the case of Ξ^- and Ω^- candidates, two other tracks projected from the chambers upstream of the first spectrometer were required to intersect to within 0.6 cm in the decay region, forming a neutral V. Where possible, tracks in the two spark-chamber clusters between the spectrometer magnets were combined so as to increase the lever arm and thus increase the accuracy of momentum determination by the spectrometers. All topologically good tracks were required to be within the over-all fiducial volume as defined by cuts near apertures and edges of the decay region.

After the vertical (non-bending-plane) constraint was used to associate track segments on either side of the spectrometer magnets, the momenta of particles which traversed the magnets were determined. Details of the momenta determination are presented elsewhere.[5] The resulting momenta as determined by the magnetic spectrometers and the beam-particle momentum as determined by the high-resolution spark chamber were used to kinematically reconstruct the events. In the case of π^- triggers, the momentum as determined by the high-resolution chamber and by the first spectrometer were required to be within 5.0 GeV/c. The events which passed these criteria were taken as the number of beam π^- detected for each run.

Σ^- triggers were reconstructed by hypothesizing the decay $\Sigma^- \rightarrow n\pi^-$. Since the momenta and directions of both the Σ^- and the decay pion candidate

are known, the kinematic fit to this hypothesis is once overconstrained, allowing the beam-particle mass to be calculated. Figure 2 depicts the reconstructed beam mass spectrum for a sample of Σ^- triggers. The mass spectrum has a width of $\sigma = 10$ MeV, and is well reproduced by Monte Carlo simulations when the effects of experimental resolution are included. This spectrum has no apparent background, so that no kinematic cuts were needed. This procedure was followed for each run to obtain the number of beam Σ^- detected.

Ξ^- and Ω^- triggers were kinematically reconstructed in two steps after the nitrous-oxide Čerenkov counter was used to separate Ω^- from Ξ^- candidates in the lengthy run at 20.5 GeV/c hyperon momentum. First, the decay Λ^0 was reconstructed from the momenta and directions of the decay tracks, with the decay hypothesized as $\Lambda^0 \rightarrow \pi^- p$. There is a twofold ambiguity in that it is not known, *a priori*, which negatively charged particle observed in the chambers surrounding the first spectrometer magnet is the π^- from the Λ^0 and is therefore the correct decay product for pairing with the proton candidate observed in both spectrometers. Both pairings were used in calculating the Λ^0 mass spectrum, which is shown in Fig. 3. The sharp peak comes from events with the correct pairing, the broad background from incorrect pairings. (It should be noted that erroneous pairing would have no effect on the Ξ^- signal because one ultimately reconstructs the $\pi^-\pi^- p$ effective mass.) The effect of mispairing on an Ω^- event would be quite small, due only to reversing the roles of π^- and K^- in reconstructing the $K^-\pi^- p$ effective mass. This effect is virtually eliminated by defining the correct pairing as that which gives an event in the Λ^0 mass peak in Fig. 3. Fewer than 5% of the events give both pairings within 5 MeV of the nominal Λ^0 mass, and in this case one pairing was chosen at random.

The second step in reconstructing Ξ^- and Ω^- candidates is to reconstruct the effective mass of all three decay tracks (hypothesized to be $\pi^-\pi^- p$ or $K^-\pi^- p$, respectively). The measured beam particle momentum for these events is ignored, leaving a once-overconstrained kinematic fit. Figure 4 depicts the reconstructed $\pi^-\pi^- p$ mass for a sample of Ξ^- triggers. The signal is very clean ($\sigma = 2$ MeV) and requires no kinematic cuts. This spectrum is well reproduced by Monte Carlo simulation. The procedure outlined above was followed in obtaining the number of detected Ξ^- for each run. The extraction of the Ω^- event is discussed below.

The second phase of the data analysis incorporated the numbers of detected events of each particle type and a Monte Carlo calculation of the detection efficiency of the apparatus and of the acceptance and decay loss in the channel to extract the relative particle production cross sections at the production target. The Monte Carlo simulation was performed for each secondary momentum. The effects of finite target size, scattering of particles in the walls of the beam channel, hyperon lifetime, geometric acceptance of the detectors, the probability of a neutron from $\Sigma^- \rightarrow n\pi^-$ convert-

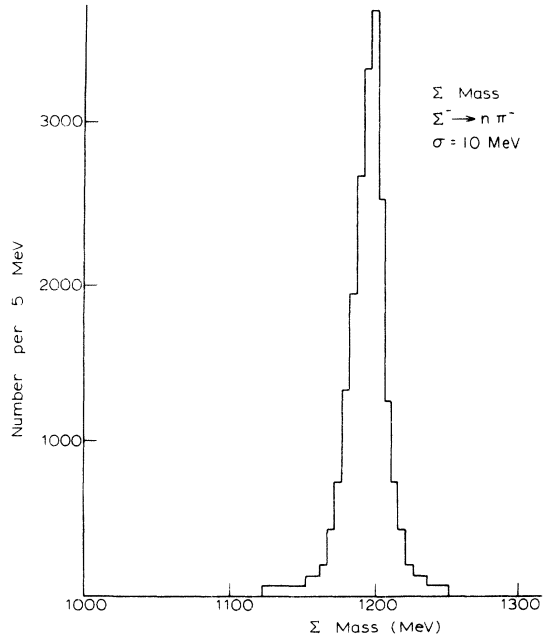

FIG. 2. Typical Σ^- reconstructed mass spectrum from $n\pi^-$ triggers.

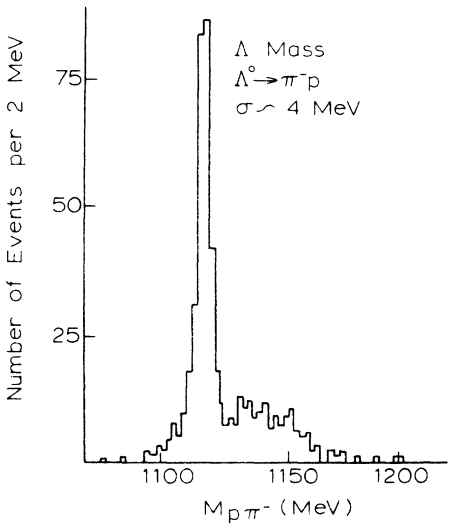

FIG. 3. Typical Λ^0 reconstructed mass spectrum from $\Lambda^0\pi^-$ triggers.
$\searrow \pi^- p$

ing in the neutron detector, finite spark-chamber resolution, and all cuts used in the analysis of the data were accounted for at each secondary momentum. The Monte Carlo calculation did not include the effects of spark-chamber inefficiency. As will be discussed below, such inefficiency is canceled in calculating the Σ^-/π^- ratio at 29.4 GeV/c incident proton momentum, but can have an effect on that ratio at 25.8 GeV/c and on the Ξ^-/π^- ratio.

V. RESULTS

The Σ^-/π^- and Ξ^-/π^- ratios at the production target as a function of secondary momentum are given in Table I. The numbers of π^- for runs with 29.4 GeV/c incident proton momentum were calculated from analyzed pion triggers, while for runs with 25.8 GeV/c proton momentum the numbers of π^- were calculated from the scaled rate of pion triggers. Figure 5 depicts the values of Σ^-/π^- and Ξ^-/π^- at the production target as a function of secondary momentum.

An empirical fit[6] to π^- production on Be was then used to calculate the absolute Σ^- and Ξ^- production cross sections at the target. These cross sections are presented in Table II. Figure 6 shows the invariant cross section for Σ^- and Ξ^- production on Be at 0°,

TABLE I. Σ^-/π^- and Ξ^-/π^- ratios at production target as a function of secondary momentum.

Σ^-/π^- production ratios for 25.8-GeV/c protons on beryllium	
Secondary momentum (GeV/c)	Σ^-/π^-
17.75	0.329 ± 0.042
18.75	0.465 ± 0.048
19.75	0.669 ± 0.067
20.75	1.08 ± 0.077
21.75	2.41 ± 0.14
22.75	2.85 ± 0.14
23.75	21.91 ± 1.4

Σ^-/π^- and Ξ^-/π^- production ratios for 29.4-GeV/c protons on beryllium

Secondary momentum (GeV/c)	Σ^-/π^-	$10^2\ \Xi^-/\pi^-$
17.0	0.185 ± 0.011	1.46 ± 0.23
19.0	0.263 ± 0.016	1.51 ± 0.16
20.0	0.374 ± 0.022	•••
20.5	0.380 ± 0.021	1.43 ± 0.11
21.0	0.463 ± 0.028	•••
22.0	0.648 ± 0.037	1.14 ± 0.10
23.45	1.19 ± 0.07	1.03 ± 0.13
25.0	1.72 ± 0.16	1.48 ± 0.22
26.0	2.62 ± 0.16	0.69 ± 0.28

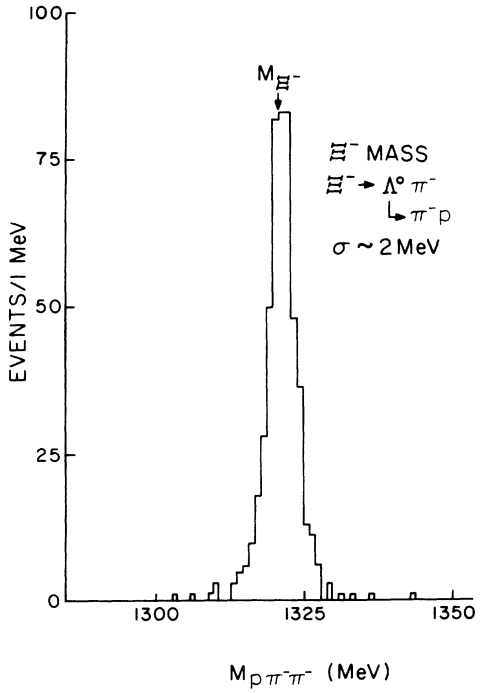

FIG. 4. Typical Ξ^- reconstructed mass spectrum from $\Lambda^0\pi^-$ triggers.
$\searrow \pi^- p$

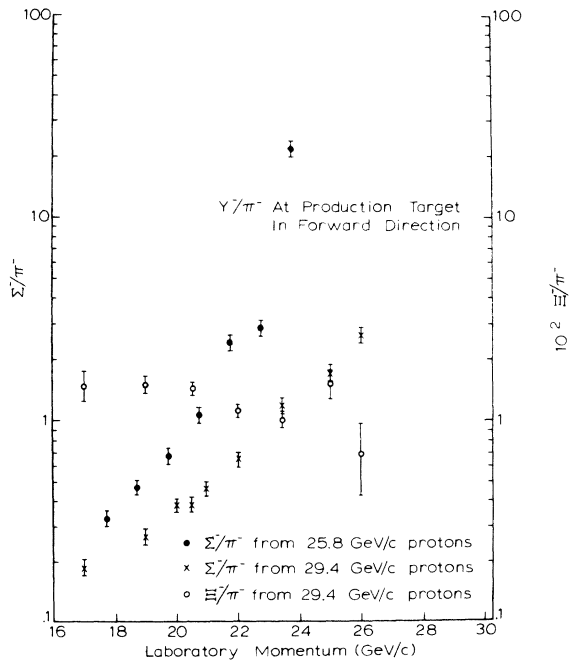

FIG. 5. Σ^-/π^- and Ξ^-/π^- production ratios in the forward direction for protons on Be.

$$E\frac{d^3\sigma}{dp^3} = \frac{E}{p^2}\frac{d^3\sigma}{dpd\Omega},$$

plotted as a function of α. Here p and E are the momentum and total energy of the produced particle, and α is its laboratory momentum normalized to the kinematic limit[7] in the reaction

$$P + \mathrm{Be} \rightarrow Y^- + \text{anything},$$

where $Y^- = \Sigma^-$ or Ξ^- as appropriate. In Fig. 6 we also plot the observed invariant cross sections for several inclusive processes

$$p + \mathrm{Be} \rightarrow C + \text{anything},$$

where $C = \pi^\pm, K^\pm, p^\pm$. Again the data are plotted with the momentum of the outgoing observed particle, C, normalized to the kinematic limit. The $\pi^\pm$, $K^\pm$, and $p^\pm$ curves are derived from the data of Allaby *et al.*[8]

A recent experiment[9] at CERN has measured Σ^- and Ξ^- production on tungsten by 24.0-GeV/c protons at a 10-mrad production angle. When corrected for the difference in production angles, the hyperon yields per nucleon measured in the CERN experiment agree with our results to within 20%.

Data from the Ω^- search at 20.5 GeV/c secondary momentum were analyzed as described above for Ξ^- and Ω^- triggers. The run yielded 8400 detected Ξ^- events and one Ω^- candidate. This single event had a reconstructed Λ^0 mass of 1113 MeV and a reconstructed $K^-\pi^-p$ mass of 1674 MeV. The summed vector momentum of the decay products was equal to that of the incident beam particle to within experimental errors. In spite of the uncertainties associated with a one-event sample, we feel that the probability of the event being due to background is rather small because the topology is that of an Ω^-, the Λ^0 and Ω^- reconstructed masses are as expected, and the summed momentum of the decay products agrees well with that measured for the incident particle. A Monte Carlo calculation was used to extract the ratio of Ω^- to Ξ^- production at the target.

On the basis of this single Ω^- candidate the production ratio of Ω^- to Ξ^- at 20.5 GeV/c secondary momentum from incident protons is

TABLE II. Σ^- and Ξ^- production cross sections at target.

Forward Σ^- production cross section for 25.8-GeV/c protons on beryllium

Secondary momentum (GeV/c)	$d^3\sigma/dPd\Omega$ [mb (sr GeV/c)$^{-1}$]
17.75	14.41 ±1.8
18.75	13.3 ±1.4
19.75	12.0 ±1.2
20.75	11.7 ±0.8
21.75	14.9 ±0.9
22.75	9.4 ±0.5
23.75	4.0 ±0.2

Forward Σ^- and Ξ^- production cross section for 29.4-GeV/c protons on beryllium

Secondary momentum (GeV/c)	$d^3\sigma/dPd\Omega$ [mb (sr GeV/c)$^{-1}$] Σ^-	Ξ^-
17.0	25.3 ± 1.5	2.00 ±0.32
19.0	19.0 ± 1.2	1.03 ±0.11
20.0	19.0 ± 1.1	•••
20.5	16.3 ± 1.0	0.620 ±0.048
21.0	16.3 ± 1.0	•••
22.0	15.3 ± 0.9	0.275 ±0.024
23.45	15.0 ± 0.9	0.131 ±0.017
25.0	10.1 ± 0.9	0.087 ±0.013
26.0	6.0 ± 0.4	0.0156 ± 0.0063

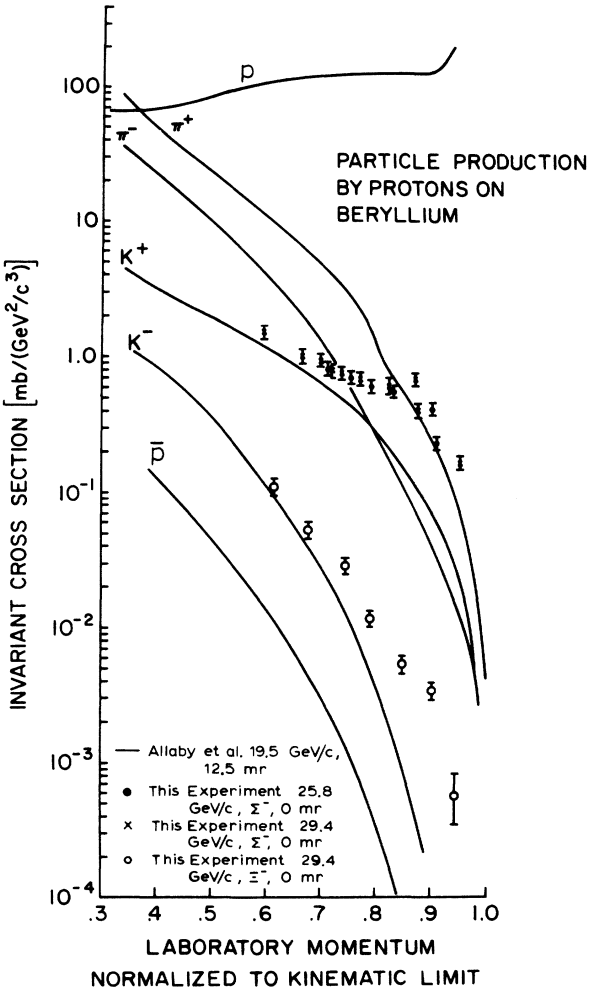

FIG. 6. The invariant inclusive cross section, $(E/p^2)(d^3\sigma/dpd\Omega)$, plotted as a function of the longitudinal laboratory momentum normalized to its kinematic limit for various particles produced in proton-Be collisions.

$$\Omega^-/\Xi^- = 1.1 \times \exp(35.6/c\tau) \times 10^{-6}$$
$$= 0.01 \quad \text{if } c\tau = 3.9 \text{ cm},$$

where τ is the Ω^- lifetime.

The errors indicated in all graphs and tables in this paper are statistical only. There are, however, several sources of possible systematic normalization errors. Uncertainties in the hyperon lifetimes and the Monte Carlo calculation of the channel and detection apparatus acceptance contribute an additional systematic uncertainty of about 15%. For the Σ^- results, uncertainties in the spark-chamber efficiencies contribute only for the 25.8-GeV/c data, where pion triggers were counted rather than analyzed. For the 29.4-GeV/c Σ^- results, the effect of possible spark-chamber inefficiency is removed by taking the Σ^--to-π^- ratio since Σ^- and π^- events are topologically equivalent. The effect of possible spark-chamber inefficiencies on the Ξ^- results is potentially more serious. The decay

$$\Xi^- \rightarrow \Lambda^0\pi^-$$
$$\qquad\searrow$$
$$\qquad\pi^-p$$

is topologically very different from beam π^-; in the spark chambers before and after the first spectrometer magnet the Ξ^- decay produces three tracks while beam pions only produce one. The spark chambers associated with the second spectrometer are generally not used to detect beam pions, while for Ξ^- decays they must detect a single track. This topological difference results in a Ξ^--to-π^- efficiency which is proportional to the product of the ratio of the triple-track to the single-track efficiencies of the chambers associated with the first spectrometer and the single-track efficiencies of those chambers associated with the second spectrometer.

The corrections for the spark-chamber inefficiencies were extracted from the data by assuming that inefficiencies were uncorrelated from chamber to chamber. Since each cluster consists of five chambers, each which determines two orthogonal coordinates, particle tracks are overconstrained in each cluster. Thus, one can determine the efficiency of each chamber in a given cluster by using the other chambers in that cluster to determine the particle trajectory.

For the 25.8-GeV/c Σ^- data this correction is negligible compared to the statistical error. A 25% correction for chamber inefficiency was applied to the Ξ^- data. This correction has the effect of increasing the observed Ξ^-/π^- ratio.

The correction for spark-chamber inefficiency has some weak dependence on secondary momentum because the flux of background particles (mostly muons from the primary proton beam dump) through the sensitive area of the spark chambers varies somewhat as the magnetic field in the beam channel is changed. We estimate the uncertainty in the efficiency correction to contribute a 10% uncertainty to the normalization for Ξ^- and a 5% uncertainty for the 25.8-GeV/c Σ^- data.

VI. DISCUSSION OF RESULTS

Our data are relevant to the question of scaling in single-particle hadron production in that we measure the invariant cross section for Σ^- production from protons on beryllium for two different proton energies (Fig. 6). Scaling in the variable α, which is essentially the Feynman scaling variable, has been verified for the production of mesons and nonstrange baryons in other experiments.[10] Within the accuracy of these measurements we feel that our two sets of data for Σ^- production are consistent with the invariant cross section scaling in the variable α. Future measurements[11] of Σ^- and Ξ^- production at higher energies will provide further tests of this scaling behavior.

An interesting feature of our data is the fact that above $\alpha = 0.75$ there are more negative hyperons than negative pions produced at 0° in proton-beryllium interactions. Such an effect can be understood in a qualitative manner by assuming that the hyperons are produced in the decay of various Y^* resonances rather than directly in the proton interactions.[12] The relatively peripheral nature of the observed Σ^- production spectrum is then a reflection of the dynamics of Y^* production in baryon-baryon interactions.

Our data may also be viewed in the context of the hypothesis of limiting fragmentation as put forth by Yang and co-workers.[14] Single-particle inclusive spectra are thought to approach their kinematic limits differently if the observed particle is favored or disfavored, i.e., depending on whether quantum numbers are changed. For $p + \text{Be} \rightarrow C + X$, C = proton is favored, while $C = \pi^+, \pi^-, K^+, K^-, \bar{p}, \Sigma^-, \Xi^-$ are disfavored. The predicted behavior is quite evident from these data. However, we note that the Σ^- spectrum of Fig. 6 displays attributes of both favored and disfavored spectra. For $\alpha < 0.9$ it is relatively flat, like the proton spectrum, while near the kinematic limit the behavior is like other disfavored distributions. Perhaps this is another reflection of the observed Σ^- spectrum having a large component derived from Y^* decay. Such effects are not seen in the Ξ^- spectrum. In any event, the simple picture of quantum number exchange determining the general feature of inclusive distributions must be modified to account for the nature of the quanta exchanged.

ACKNOWLEDGMENTS

We wish to thank our engineering staff, Satish Dhawan, Andy Disco, Cordon Kerns, Blaise Lombardi, and Irving Winters, and our technicians, Jon Blomquist, Ed Steigmeyer, and Alan Wandersee, for their help in the design and setup of the apparatus. We also thank the AGS staff, in particular David Berley, for providing the technical support needed for the success of this experiment. The proton calorimeter was graciously provided by the University of Pittsburgh group.

---

*Research supported by the U. S. Atomic Energy Commission under Contract No. AT(11-1)3075.

†Present address: Université de Genève, Switzerland.

‡Present address: SLAC, Stanford, California.

§Present address: CERN, Geneva, Switzerland.

||Operated by Universities Research Association Inc. under contract with the U. S. Atomic Energy Commission.

¶Work supported by the U. S. Atomic Energy Commission.

[1]Results describing Σ^- production in proton-beryllium interactions were reported by V. Hungerbühler *et al.*, Phys. Rev. Lett. 30, 1234 (1973).

[2]V. Hungerbühler *et al.*, Nucl. Instrum. Methods 115, 221 (1974).

[3]The chemical composition of Freon 13 Bl is $CBrF_3$.

[4]W. J. Willis *et al.*, Nucl. Instrum. Methods 91, 33 (1971).

[5]W. M. Tanenbaum, thesis, Yale University, 1974 (unpublished).

[6]C. L. Wang, Phys. Rev. Lett. 25, 1068 (1970).

[7]The kinematic limit was calculated by separately considering proton and neutron targets and averaging the respective kinematic limits. For $p+p \rightarrow \Sigma^- + X$, for example, X = proton + pion + kaon, while for $p+n \rightarrow \Sigma^- + X$, X = proton + pion.

[8]J. V. Allaby *et al.*, CERN Report No. 70-12, 1970 (unpublished).

[9]J. Badier *et al.*, Phys. Lett. 39B, 414 (1972).

[10]T. Ludlam *et al.*, LBL Report No. LBL-80, 1972 (unpublished).

[11]Yale-NAL Collaboration, NAL Proposal 97 (unpublished).

[12]Yale-NAL-BNL Collaboration, AGS Proposal 430 (unpublished).

[13]J. Benecke *et al.*, Phys. Rev. 188, 2159 (1969).

[14]T.T. Chou and C. N. Yang, Phys. Rev. Lett. 25, 1072 (1970).